Three-Phase Interleaved LLC Asymmetric Resonant Converter With Capacitive Current Balancing and Reduced Switch Voltage Stress

YOSHIYA TADA[1], (Student Member, IEEE), MASATOSHI UNO[1], (Member, IEEE), AND YUSUKE SATO[2]

[1]Graduate School of Science and Engineering, Ibaraki University, Hitachi 316-8511, Japan
[2]Panasonic Corporation, Yokohama 224-8520, Japan

Corresponding author: Masatoshi Uno (masatoshi.uno.ee@vc.ibaraki.ac.jp)

ABSTRACT Interleaved converters are a typical solution to enhance a current capacity and to reduce current ripples of an input or output port. Conventional interleaved LLC resonant converters need additional switches and passive components with a feedback control loop for active current balancing, increasing the circuit complexity and cost. This paper proposes a novel three-phase interleaved LLC resonant converter with an automatic capacitive current balancing capability. Two flying capacitors are added to a conventional interleaved LLC resonant converter in order to realize not only the automatic capacitive current balancing but also the reduced switch voltage stresses and asymmetric resonant operations that contribute to reducing rms currents as well as copper losses of transformers. The detailed operation analysis, including the capacitive current balancing mechanism and gain characteristics derivation, are performed. The experimental verification using a 1-kW prototype demonstrated that the automatic capacitive current balancing could be achieved despite the significant mismatch in transformers' parameters.

INDEX TERMS Asymmetric resonance, current balancing, flying capacitor, interleaved converter, LLC resonant converter.

I. INTRODUCTION

Interleaved converters consisting of parallel-connected multiple converters operating out of phase at the same frequency are widely used to enhance a current capacity and to reduce current ripples of an input or output port. Gain characteristics of parallel-connected phases are naturally mismatched to a certain degree due to component tolerance. Currents flowing through each phase (hereafter call 'phase currents') are imbalanced due to the gain characteristic mismatch, causing a current concentration and increased current stresses. To balance phase currents in the interleaved PWM converters, all phase currents are measured, and a duty cycle of each phase is individually adjusted so that the gain characteristics of parallel-connected phases are matched [1]. This active current balancing technique, however, requires not only multiple current sensors but also an additional current balancing feedback

control loops, resulting in increased circuit complexity and cost.

A previous work [2] has proposed an automatic current balancing technique based on a magnetic coupling. Topologies employing a magnetic coupling for the current balancing are prone to be bulky due to a large number of magnetic components. An interleaved PWM buck and boost converters presented in [3], [4] realize an automatic capacitive current balancing thanks to the charge conservation of dc blocking capacitors. In this interleaved buck converter, the number of phases can be extended without impairing the automatic current balancing capability.

Meanwhile, LLC resonant converters offer prominent features of galvanic isolation, high efficiency, high-power density, and reduced switching loss and EMI thanks to zero voltage switching (ZVS) operations. In general, gain characteristics of LLC resonant converters are dependent on their frequency-dependent impedance characteristics, suggesting that switching frequencies of parallel-connected LLC resonant converters need to be individually adjusted

to balance phase currents. Alternatively phrased, parallel-connected LLC resonant converters eventually operate at different switching frequencies [5], [6], and therefore, interleaving operations cannot be simply applied to LLC resonant converters.

Several interleaved LLC resonant converters with active current balancing techniques have been proposed [7]–[9]. The interleaved LLC resonant converter presented in [7] adds variable inductors in order to compensate gain characteristic mismatches. Topologies proposed in [8] and [9] adjust parasitic capacitances of MOSFETs by controlling their switching frequencies, but the slight mismatch in a resonant capacitance (e.g., 5%) reportedly results in the existence of phases no longer contributing to power conversion. In general, interleaved LLC resonant converters with an active current balancing are prone to be complex and costly due to additional feedback control loops and current sensors for the active current balancing.

The multi-phase LLC resonant converters presented in [10]–[13], on the other hand, achieve a passive current balancing without additional feedback control loops nor current sensors, but there are still challenges to be addressed. Topology reported in [10] cannot achieve adequate current balancing if the transformers' parameters are mismatched. The interleaved LLC resonant converter employing common inductors tends to suffer from a current imbalance under light load conditions [11]. The three-phase interleaved LLC resonant converter developed in [12] automatically balances three-phase currents by utilizing an integrated transformer and current balancing transformer. However, the existence of the integrated transformer not only increases its design difficulty but also impairs the LLC resonant converters' advantage of the simple structure. Meanwhile, the two-phase interleaved LLC resonant converter [13] achieves an automatic capacitive current balancing thanks to the charge conservation of a capacitor even under light load conditions, but output current ripples cannot be reduced even with the interleaving structure. In addition, a three-phase LLC resonant converter topology with capacitive current balancing has not been proposed yet.

This paper proposes a novel three-phase interleaved LLC resonant converter with an automatic capacitive current balancing capability. Two flying capacitors are added to a conventional three-phase LLC resonant converter to realize not only the automatic capacitive current balancing but also reduced switch voltage stresses. In addition, the added flying capacitors achieve asymmetric resonant operations, by which rms currents of resonant tanks in the case of asymmetric duty cycles $d \neq 0.5$ can be reduced.

This paper is organized as follows. Section II introduces the proposed three-phase interleaved LLC asymmetric resonant converter and its major features. Section III explains the mechanisms of the automatic capacitive current balancing and asymmetric resonant operation. The operation analysis, switch voltage stress, and gain characteristics will be discussed in detail in Section IV. The experimental verification using a 1-kW prototype will be presented in Section V.
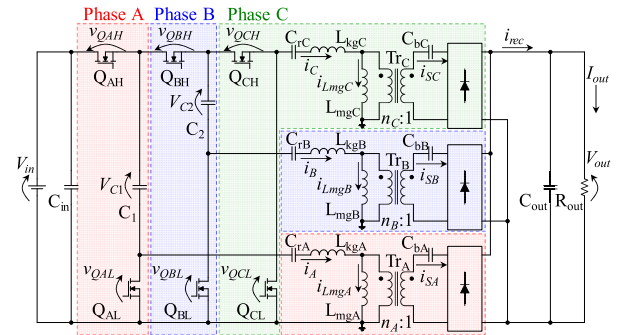

FIGURE 1. Proposed three-phase interleaved LLC asymmetric resonant converter.

II. PROPOSED THREE-PHASE INTERLEAVED LLC ASYMMETRIC RESONANT CONVERTER

A. CIRCUIT DESCRIPTION

Figure 1 illustrates the proposed three-phase interleaved LLC resonant converter. The circuit on the transformers' primary side consists of three LLC resonant tanks, three switching legs, and two flying capacitors C_1 and C_2—subscript symbols of A–C correspond to Phases A–C. C_1 and C_2 are inserted between high- and low-side switches of Phases A and B (i.e., Q_{AH} and Q_{AL}, and Q_{BH} and Q_{BL}), respectively. On the transformers' secondary side, full-wave rectifiers, each containing a dc blocking capacitor C_{bA}–C_{bC} to prevent dc bias currents of transformers, are connected in parallel.

Three pairs of high- and low-side switches (Q_{jH} and Q_{jL}, where j is A, B, or C) are driven in a complementary mode, and these three switching legs operate in an interleaving manner of 120° out of phase. Duty cycles d of high-side switches (Q_{jH}) are fixed to be 0.33 for the interleaving operations and automatic current balancing. C_1 and C_2 realize not only an automatic capacitive current balancing but also reduced voltage stresses of switches. Furthermore, C_1 and C_2 also take part in the asymmetric LLC resonant operations that are suitable operation modes for resonant converters operating with asymmetric duty cycles (i.e., $d \neq 0.5$), as will be detailed in Section III-B.

B. BENEFITS AND DRAWBACKS

Even if component parameters among three phases are mismatched, the phase currents i_j are automatically balanced without feedback control loops nor current sensors thanks to the charge conservation of C_1 and C_2, as will be discussed in Section III-A. Therefore, the proposed interleaved LLC resonant converter can reduce circuit complexity and cost compared with conventional topologies relying on active current balancing techniques [5]–[9].

Switches in traditional LLC resonant converters must be rated for a full input voltage V_{in}. In the proposed interleaved LLC converter, on the other hand, flying capacitors, C_1 and C_2, contribute to reducing the switches' voltage stresses lower than two-third of the input voltage, as will be detailed in Section IV-B. The reduced voltage stresses translate to lower on-resistances, eventually reducing conduction losses.

The proposed interleaved LLC converter adopts the asymmetric resonant operation by employing C_1 and C_2 for resonance. The asymmetric resonant operation reduces rms current as well as Joule losses of components and copper losses of the transformers compared with those in the conventional interleaved LLC converter operating with the symmetric resonance.

The number of phases in the proposed interleaved converter can be extended to increase the current capacity of the converter. However, capacitances of flying capacitors need to be properly designed to achieve the asymmetric resonant operations, resulting in increased design difficulty of the resonant tanks compared with the ordinary LLC resonant converters, as will be detailed in Section III-B. Given the design difficulty of the asymmetric resonant tanks in extended topologies, three- or four-phase topologies would be the practical implementation of the proposed interleaved LLC converter.

Similar to the ordinary LLC resonant converters, the output voltage of the proposed converter is regulated by pulse frequency modulation (PFM) control. All switches in the proposed converter achieve ZVS turn-on and -off by utilizing magnetizing inductances of transformers, L_{mgj}, and parasitic capacitances of MOSFETs, C_{OSS}. All the diodes on the transformers' secondary side achieve zero current switching (ZCS) turn-on and -off.

Since the proposed converter operates with the asymmetric duty cycle of $d \neq 0.5$, dc blocking capacitors of C_{bj} are necessary to prevent magnetic saturation of the transformer.
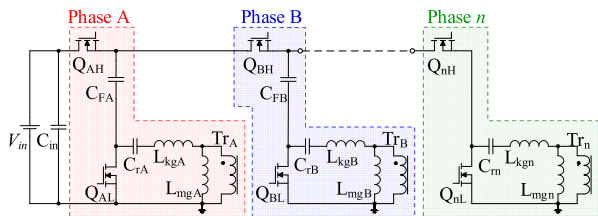

FIGURE 2. Concept of extension for multi-phase interleaved LLC resonant converter.

C. EXTENSION TO MULTIPLE PHASE

The concept of the proposed interleaved LLC converter can be extended to arbitrary numbers of phases. The generalized concept of the proposed multi-phase interleaved converter is shown in Fig. 2. The transformers' secondary sides are not illustrated for the sake of clarity. The number of phases can be arbitrarily increased by adding the circuit consisting of a resonant tank, two switches, and a flying capacitor. Extended topologies of the multi-phase interleaved LLC converter also achieves an automatic current balancing, reduced switches' voltage stresses, and asymmetric resonant operations thanks to the flying capacitors.

Resonant frequencies need to be properly designed with considering asymmetric duty cycles, as will be explained in the next section. Let n be the number of phases, duty cycles d

of high-side switches are $1/n$. Therefore, the larger the number of phases, the smaller will be the duty cycles, resulting in increased design difficulties of asymmetric resonant frequencies. Accordingly, three- or four-phase topologies would be practical from the viewpoint of design difficulty.
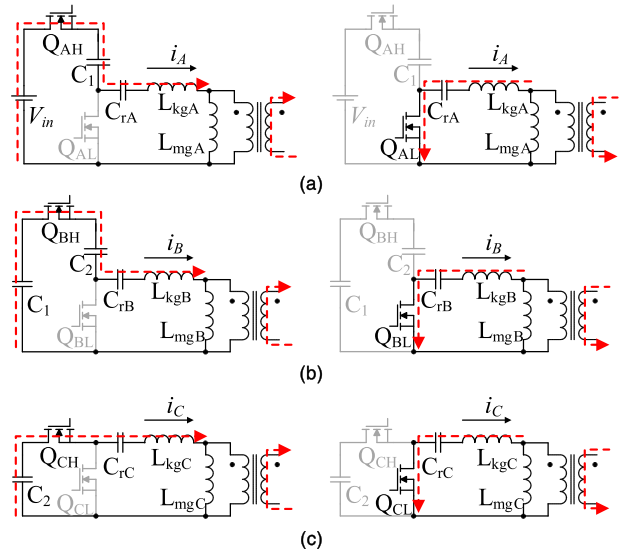

FIGURE 3. Current flows in (a) Phase A, (b) Phase B, and (c) Phase C.

III. AUTOMATIC CAPACITIVE CURRENT BALANCING AND ASYMMETRIC RESONANT OPERATION

A. AUTOMATIC CAPACITIVE CURRENT BALANCING

The proposed converter offers an automatic current balancing owing to the charge conservation of flying capacitors of C_1 and C_2. The current flows in each phase are highlighted in Fig. 3. As shown in Fig. 3(a), during the period when i_A is positive, C_1 and C_{rA} in the resonant tank of Phase A are charged in series. In the period when C_1 is discharging, C_2 and C_{rB} in the resonant tank of Phase B are charged in series by C_1, as shown in Fig. 3(b). In summary, C_1 is charged together with C_{rA} of Phase A, and C_1 discharges to C_2 and C_{rB} of Phase B. Therefore, the phase currents of i_A and i_B are automatically balanced by the charge conservation of C_1. After C_2 is charged with C_{rB} in the resonant tank of Phase B, C_2 discharges to C_{rC} in the resonant tank of Phase C, as illustrated in Fig. 3(c). Hence, the phase currents of i_B and i_C are naturally balanced by C_2. Consequently, all phase currents are automatically balanced thanks to C_1 and C_2 even if component parameters are mismatched.

B. ASYMMETRIC RESONANT OPERATION

In general, to improve the power conversion efficiency of traditional LLC converters operating with a symmetric duty cycle of $d = 0.5$, rms currents at a given output power need to be minimized with ensuring ZVS operations. To this end, the resonant period $1/f_r$ is set to be slightly shorter than the switching period T_S. The proposed interleaved LLC converter, on the other hand, operates with an asymmetric

duty cycle of $d = 0.33$ for high-side switches, and hence, positive and negative half resonant periods, $1/2f_{rP}$ and $1/2f_{rN}$, must be shorter than $T_S/3$ and $2T_S/3$, respectively.
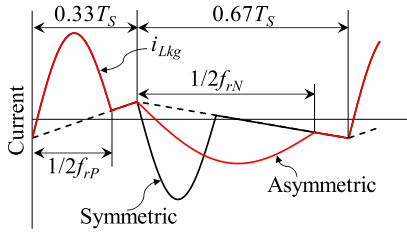

FIGURE 4. Current waveforms of symmetric and asymmetric LLC resonances.

Figure 4 compares the current waveforms of the symmetric and asymmetric resonant operations with $d = 0.33$. The resonant frequencies of the positive half cycle are identical. In the negative half cycle, the negative peak current of the asymmetric resonance is reduced compared with that of the symmetric resonance. Thus, the asymmetric resonant operations can lower negative peak currents, reducing rms currents as well as conduction losses.

As shown in Fig. 3, in the positive half cycle of resonance, not only the resonant tanks but also the flying capacitors of C_1 and C_2 take part in the resonant operations. The resonant frequencies of positive and negative half cycles of Phases A–C, $f_{rAP} - f_{rCP}$ and $f_{rAN} - f_{rCN}$, are expressed as

$$f_{rAP} = \frac{1}{2\pi \sqrt{L_{kgA} \frac{C_1 C_{rA}}{C_1 + C_{rA}}}} \tag{1}$$

$$f_{rAN} = \frac{1}{2\pi \sqrt{L_{kgA} C_{rA}}} \tag{2}$$

$$f_{rBP} = \frac{1}{2\pi \sqrt{L_{kgB} \frac{C_1 C_2 C_{rB}}{C_1 C_2 + C_2 C_{rB} + C_{rB} C_1}}} \tag{3}$$

$$f_{rBN} = \frac{1}{2\pi \sqrt{L_{kgB} C_{rB}}} \tag{4}$$

$$f_{rCP} = \frac{1}{2\pi \sqrt{L_{kgC} \frac{C_2 C_{rC}}{C_2 + C_{rC}}}} \tag{5}$$

$$f_{rCN} = \frac{1}{2\pi \sqrt{L_{kgC} C_{rC}}}. \tag{6}$$

$f_{rAN} - f_{rCN}$ are written in the identical form as that of traditional LLC converters. $f_{rAP} - f_{rCP}$, on the other hand, are dependent on not only parameters of the resonant tanks but also C_1 and C_2. Properly designing C_1 and C_2 can reduce rms currents as well as conduction losses.

Assume $L_{kgA} = L_{kgB} = L_{kgC} = L_{kg}$ and $C_{rA} = C_{rB} = C_{rC} = C_r$, the resonant frequency of negative half cycle, f_{rN}, is expressed as

$$f_{rN} = \frac{1}{T_{rN}} = f_{rAN} = f_{rBN} = f_{rCN} = \frac{1}{2\pi \sqrt{L_{kg} C_r}} \tag{7}$$

where T_{rN} is the resonant period of the negative half cycle. Let $C_1 = C_2 = C_f$, the resonant frequency of positive half

cycles, f_{rP}, and f_{rBP} are represented as

$$f_{rP} = \frac{1}{T_{rP}} = f_{rAP} = f_{rCP} = \frac{1}{2\pi \sqrt{L_{kg} \frac{C_f C_r}{C_f + C_r}}} \tag{8}$$

$$f_{rBP} = \frac{1}{2\pi \sqrt{L_{kg} \frac{C_f C_r}{C_f + 2C_r}}} \tag{9}$$

where T_{rP} is the resonant period of the positive half cycle.

f_{rAP} and f_{rCP} are expressed in the identical form, whereas f_{rBP} is slightly higher. C_1 and C_2 should desirably be determined so that $f_{rAP} \approx f_{rBP}$ to equalize peak currents of Phases A–C. Meanwhile, because the proposed interleaved LLC converter operates with the asymmetric duty cycle of $d = 0.33$, f_{rP} and f_{rN} are preferably designed to be $f_{rP} : f_{rN} = 2 : 1$.
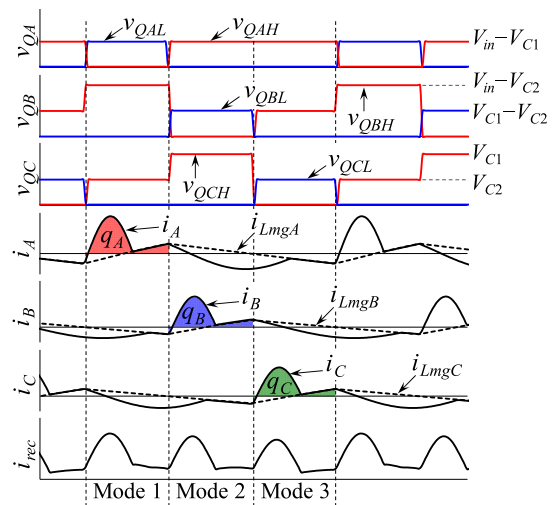

FIGURE 5. Theoretical key operation waveforms.

IV. OPERATION ANALYSIS

As discussed in Section II-A, duty cycles d of high-side switches (Q_{jH}) are fixed to be 0.33. Theoretical operational waveforms and current flows are shown in Figs. 5 and 6, respectively. To simplify the analysis, all the circuit elements are assumed ideal, and the voltages across C_1 and C_2, V_{C1} and V_{C2}, are assumed constant, though C_1 and C_2 are designed to take part in the resonant operations. Similar to traditional LLC converters, all switches and diodes achieve ZVS and ZCS, respectively. In this paper, operations during dead-time periods are omitted to save page length, and the detailed ZVS and ZCS principles are not described. The operations on the transformers' secondary sides are also omitted.

A. MODE ANALYSIS

The operation is roughly divided into three modes based on switching states.

Mode 1 [Fig. 6(a)]: This mode corresponds to the positive half cycle of Phase A, while Phases B and C are in the negative half cycles of resonant operations. C_1 and the resonant
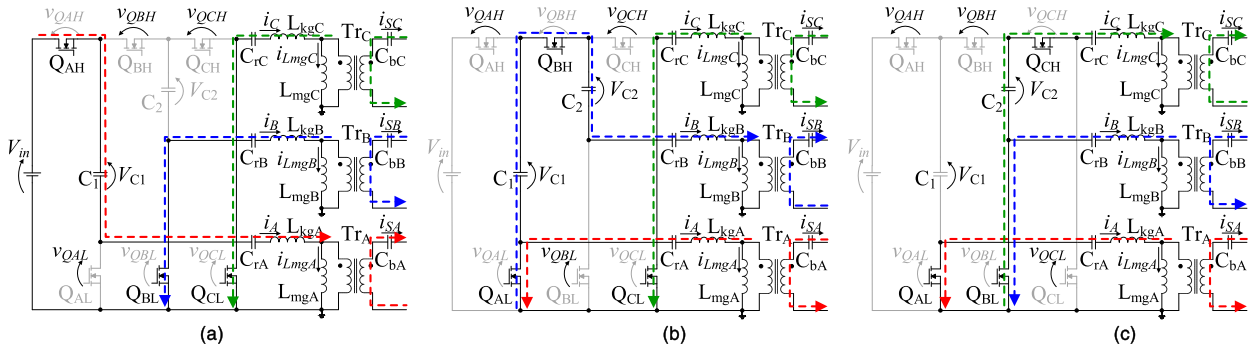
FIGURE 6. Current flows of the proposed interleaved LLC resonant converter in (a) Mode 1, (b) Mode 2, and (c) Mode 3.

tank of Phase A are charged in series with C_{rA}. The charge stored in C_1 and C_{rA} in this mode is designated as q_A (see Fig. 5). The voltages across Q_{AL}, Q_{BH}, and Q_{CH} are yielded as

$$v_{QAL} = V_{in} - V_{C1} \tag{10}$$
$$v_{QBH} = V_{in} - V_{C2} \tag{11}$$
$$v_{QCH} = V_{C2}. \tag{12}$$

Mode 2 [Fig. 6(b)]: Phases A and C operate in negative half cycles, while Phase B in the positive half cycles. In Phase B, both C_1 and C_2 take part in the resonant operation. The amount of charge stored in C_2 and C_{rB} designated as q_B (see Fig. 5) must be equal to q_A because of the charge conservation of C_1. Consequently, currents of Phases A and B, i_A and i_B, are automatically balanced. The voltage stresses of Q_{AH}, Q_{BL}, and Q_{CH} are expressed as

$$v_{QAH} = V_{in} - V_{C1} \tag{13}$$
$$v_{QBL} = V_{C1} - V_{C2} \tag{14}$$
$$v_{QCH} = V_{C1}. \tag{15}$$

Mode 3 [Fig. 6(c)]: Phases A and B are in negative half cycles, while Phase C is in a positive half cycle. C_2 participates in the resonant operation of Phase C. The released charge amount of C_2, q_C, must be equal to q_B, resulting in an automatic current balancing between Phases B and C. The voltages across Q_{AH}, Q_{BH}, and Q_{CL} can be expressed as

$$v_{QAH} = V_{in} - V_{C1} \tag{16}$$
$$v_{QBH} = V_{C1} - V_{C2} \tag{17}$$
$$v_{QCL} = V_{C2}. \tag{18}$$

B. VOLTAGE STRESSES OF FLYING CAPACITORS AND SWITCHES

The resonant tanks of Phases A–C are assumed identical, and they operate with the same duty cycles of $d = 0.33$. The voltages applied to resonant tanks of Phases A–C are equivalent to the low-side switch voltages obtained in (10), (14), and (18), respectively. Hence, average voltages of the resonant tank (or resonant capacitor) of each phase, $V_{rA} - V_{rC}$,

are expressed as

$$V_{rA} = (V_{in} - V_{C1})/3 \tag{19}$$
$$V_{rB} = (V_{C1} - V_{C2})/3 \tag{20}$$
$$V_{rC} = V_{C2}/3. \tag{21}$$

$V_{rA} - V_{rC}$ can be assumed to be identical when resonant tanks' parameters are ideally matched. Thereby, applying $V_{rA} = V_{rB} = V_{rC}$ to (19), (20), and (21) yields switch voltage stresses as

$$V_{QBH} = V_{QCH} = 2V_{in}/3 \tag{22}$$
$$V_{QAH} = V_{QAL} = V_{QBL} = V_{QCL} = V_{in}/3. \tag{23}$$

Switch voltage stresses in the proposed interleaved LLC resonant converter are one-third or two-third of V_{in}, whereas those in traditional LLC resonant converters are V_{in}. The reduced voltage stresses translate to lowered on-resistances of MOSFETs as well as reduced conduction losses.

C. GAIN CHARACTERISTICS

First harmonic approximation (FHA) is a widely used method to briefly analyze the gain characteristics of LLC resonant converters [14], [15]. However, FHA cannot be applied to the proposed interleaved LLC converter due to asymmetric duty cycles and asymmetric resonant operations. This section reveals the gain characteristics of the proposed converter by applying the time-domain analysis [16], [17]. As discussed in Section III-B, f_{rP} and f_{rN} are preferably designed to be $f_{rP} : f_{rN} = 2 : 1$ because the proposed converter operates with the asymmetric duty cycle $d = 0.33$. However, to derive the universal gain characteristics, the time-domain analysis under the condition of $f_{rAP} : f_{rAN} \neq 2 : 1$ is performed in this section.

The time-domain analysis is performed based on the following premises in order to simplify the analysis. All the circuit elements are ideal. V_{C1}, V_{C2}, and voltages across the dc blocking capacitors on the transformers' secondary sides, $V_{CbA} - V_{CbC}$, are constant. In this paper, the time-domain analysis for Phase A only is performed to save the page length, but Phases B and C can be analyzed in the same manner.

The voltage of C_{rA}, v_{CrA}, i_A, i_{LmgA}, and the current flowing through the secondary winding, i_{SA}, are highlighted in Fig. 7.
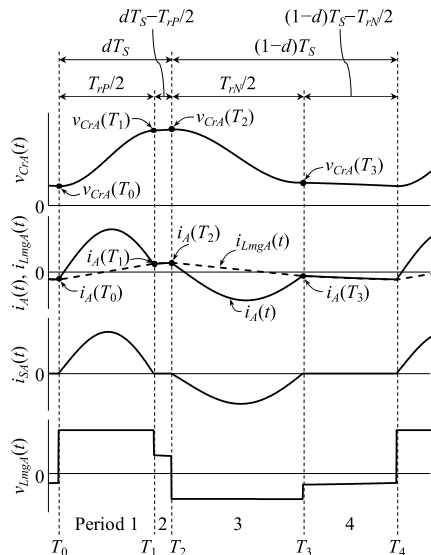
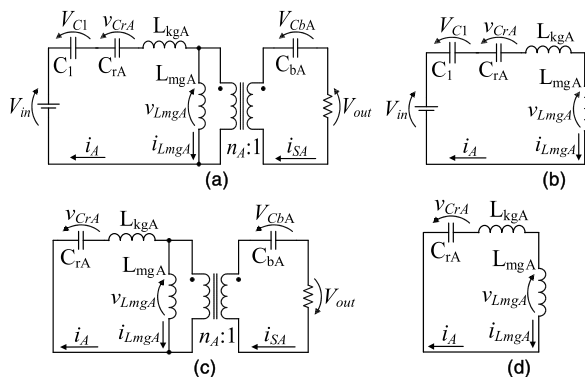**FIGURE 7.** Voltage and current waveforms in Phase A.

FIGURE 8. Equivalent circuits of Phase A: (a) Period 1, (b) Period 2, (c) Period 3, and (d) Period 4.

One switching cycle is subdivided into four periods, and equivalent circuits of Phase A in each period are illustrated in Fig. 8. Before detailing the gain characteristic analysis, V_{CbA} is derived. The voltage across L_{mgA} in Periods 1–4 is yielded as

$$
v_{Lmg} = \begin{cases} n_A (V_{CbA} + V_{out}) & \text{(Period 1)} \\ V_{in} - V_{C1} - V_{CrA.ave2} & \text{(Period 2)} \\ n_A (V_{CbA} - V_{out}) & \text{(Period 3)} \\ V_{CrA.ave4} & \text{(Period 4)} \end{cases} \tag{24}
$$

where $V_{CrA.ave2}$ and $V_{CrA.ave4}$ are the average voltages of C_{rA} in Periods 2 and 4, respectively. Equation (25), as shown at the bottom of this page, is derived from the volt-second balance on L_{mgA}, and V_{CbA} can be obtained as (26), as shown at the bottom of this page.

The characteristic impedance, Z_r, is defined as

$$
Z_r = \sqrt{\frac{L_{kgA}}{C_{rA}}}. \tag{27}
$$

Period 1 ($T \leq t \leq T_1$) [Fig. 8(a)]: C_1, C_{rA}, and L_{kgA} resonate. i_A sinusoidally changes, whereas i_{LmgA} linearly increases. v_{CrA}, i_A, and i_{LmgA} are yielded as

$$
\begin{aligned}
v_{CrA}(t) &= \{v_{CrA}(T_0) - V_{in} + V_{C1} + n_A(V_{CbA} + V_{out})\} \\
&\quad \cdot \cos\{\omega_{rAP}(t - T_0)\} + i_A(T_0) Z_r \sin\{\omega_{rAP}(t - T_0)\} \\
&\quad + V_{in} - V_{C1} - n_A(V_{CbA} + V_{out}) \tag{28}
\end{aligned}
$$

$$
\begin{aligned}
i_A(t) &= i_A(T_0) \cos\{\omega_{rAP}(t - T_0)\} \\
&\quad - \frac{v_{CrA}(T_0) - V_{in} + V_{C1} + n_A(V_{CbA} + V_{out})}{Z_r} \\
&\quad \cdot \sin\{\omega_{rAP}(t - T_0)\} \tag{29}
\end{aligned}
$$

$$
i_{LmgA}(t) = \frac{n_A(V_{CbA} + V_{out})}{L_{mgA}}(t - T_0) + i_A(T_0) \tag{30}
$$

where $\omega_{rAP} = 2\pi f_{rAP}$

Period 2 ($T_1 \leq t \leq T_2$) [Fig. 8(b)]: L_{mgA} takes part in the resonance. i_A increases together with i_{LmgA}. v_{CrA}, i_A, and i_{LmgA} are expressed as

$$
\begin{aligned}
v_{CrA}(t) &= \{v_{CrA}(T_1) - V_{in} + V_{C1}\} \cos\{\omega_{mAP}(t - T_1)\} \\
&\quad + i_A(T_1) Z_r \sqrt{1 + m} \sin\{\omega_{mAP}(t - T_1)\} + V_{in} - V_{C1} \tag{31}
\end{aligned}
$$

$$
\begin{aligned}
i_A(t) &= i_A(T_1) \cos\{\omega_{mAP}(t - T_1)\} \\
&\quad - \frac{v_{CrA}(T_1) - V_{in} + V_{C1}}{Z_r \sqrt{1 + m}} \sin\{\omega_{mAP}(t - T_1)\} \tag{32}
\end{aligned}
$$

$$
i_{LmgA}(t) = i_A(t) \tag{33}
$$

where $m = L_{mgA}/L_{kgA}$, and $\omega_{mAP} = \omega_{rAP}/\sqrt{1 + m}$.

Period 3 ($T_2 \leq t \leq T_3$) [Fig. 8(c)]: C_{rA} and L_{kgA} are resonating. i_A sinusoidally changes, and i_{LmgA} linearly decreases. v_{CrA}, i_A, and i_{LmgA} are expressed as

$$
\begin{aligned}
v_{CrA}(t) &= \{v_{CrA}(T_2) + n_A(V_{CbA} - V_{out})\} \\
&\quad \cdot \cos\{\omega_{rAN}(t - T_2)\} + i_A(T_2) Z_r \\
&\quad \cdot \sin\{\omega_{rAN}(t - T_2)\} - n(V_{CbA} - V_{out}) \tag{34}
\end{aligned}
$$

$$
\begin{aligned}
i_A(t) &= i_A(T_2) \cos\{\omega_{rAN}(t - T_2)\} \\
&\quad - \frac{v_{CrA}(T_2) + n_A(V_{CbA} - V_{out})}{Z_r} \sin\{\omega_{rAN}(t - T_2)\} \tag{35}
\end{aligned}
$$

$$
i_{LmgA}(t) = \frac{n_A(V_{CbA} - V_{out})}{L_{mgA}}(t - T_2) + i_A(T_2) \tag{36}
$$

where $\omega_{rAN} = 2\pi f_{rAN}$

$$
\begin{aligned}
&n_A(V_{CbA} + V_{out}) T_{rP}/2 + (V_{in} - V_{C1} - V_{CrA.ave2})\{dT_S - T_{rP}/2\} \\
&\quad + n_A(V_{CbA} - V_{out}) T_{rN}/2 + V_{CrA.ave4}\{(1 - d)T_S - T_{rN}/2\} = 0 \tag{25}
\end{aligned}
$$

$$
V_{CbA} = -\frac{(V_{in} - V_{C1} - V_{CrA.ave2}) T_{rP} + V_{CrA.ave4}\{2(1 - d)T_S - T_{rN}\} + n_A V_{out}(T_{rP} - T_{rN})}{n_A(T_{rP} + T_{rN})}. \tag{26}
$$

TABLE 1. Component values used for gain characteristics analysis.

Components	Value
C_1 and C_2	1.0 μF
C_{rA}–C_{rC}	680 nF
L_{kgA}–L_{kgC}	2.0 μH
L_{mgA}–L_{mgC}	30 μH
n_A–n_C	1.0
f_{rAP}–f_{rCP}	f_{rAP} = 177 kHz, f_{rBP} = 210 kHz, f_{rCP} = 177 kHz
f_{rAN}–f_{rCN}	f_{rAN} = 136 kHz, f_{rBN} = 136 kHz, f_{rCN} = 136 kHz

Period 4 ($T_3 \leq t \leq T_4$) [Fig. 8(d)]: L_{mgA} participates in the resonance. Similar to Period 2, i_A sinusoidally changes together with i_{LmgA}. v_{CrA}, i_A, and i_{LmgA} are given by

$$v_{CrA}(t) = v_{CrA}(T_3) \cos\{\omega_{mAN}(t - T_3)\}$$
$$+ i_A(T_3) Z_r \sqrt{1 + m} \sin\{\omega_{mAN}(t - T_3)\} \quad (37)$$

$$i_A(t) = i_A(T_3) \cos\{\omega_{mAN}(t - T_3)\}$$
$$- \frac{v_{CrA}(T_3)}{Z_r \sqrt{1 + m}} \sin\{\omega_{mAN}(t - T_3)\} \quad (38)$$

$$i_{LmgA}(t) = i_A(t) \quad (39)$$

where $\omega_{mAN} = \omega_{rAN} / \sqrt{1 + m}$.

As discussed in Section III-B, the resonant frequency of the positive half cycle of Phase B (i.e., f_{rBP}) differs from those of Phases A and C ($f_{rP} = f_{rAP} = f_{rCP}$). The time-domain equations for Phase B can be obtained and expressed in a similar way as (24)−(39).

Assuming Phases A and C have the identical characteristics, the gain G of the proposed three-phase interleaved LLC converter is derived as

$$G = \frac{n_A V_{out}}{V_{in}}$$
$$= \frac{n_A^2 R_{out}}{V_{in} T_S} \left(2 \int_0^{T_S} |i_A - i_{LmgA}| \, dt + \int_0^{T_S} |i_B - i_{LmgB}| \, dt \right)$$
$$\quad (40)$$

where R_{out} is the load resistance, and T_S (= $1/f_S$) is the switching period.

Theoretical and simulated characteristics of G are compared in Fig. 9, and component values used for the analysis are listed in Table 1. The normalized frequency F and quality factor Q are defined as

$$F = \frac{f_S}{f_{rAN}} \quad (41)$$

$$Q = \frac{\pi^2 \cdot Z_r}{8 n_A^2 \cdot R_{out}}. \quad (42)$$

In general, G of conventional half-bridge LLC converters converges to 0.5 at normalized frequency $F = 1.0$. Meanwhile, G of the proposed interleaved converter ideally converges to 0.167 when C_1 and C_2 are designed to be f_{rAP} : f_{rAN} = 2 : 1 because V_{C1} is $2V_{in}/3$, as discussed in Section IV-B. However, G in Fig. 9 converged to 0.17 at
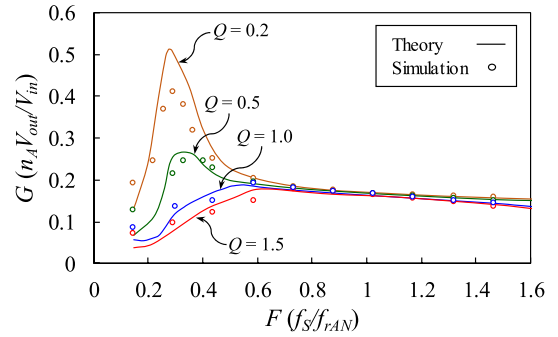

FIGURE 9. Theoretical and simulated gain characteristics.

$F = 0.9$ because C_1 and C_2 were chosen so that $f_{rAP}/f_{rAN} < 2$ in this analysis.

Theoretical and simulated characteristics agreed satisfactorily, but there were slight mismatches observed in the low-frequency region. These mismatches were due to the discrepancy between the ideal analysis and reality. The analysis was performed assuming that V_{C1} and V_{C2} are constant. In reality, however, V_{C1} and V_{C2} fluctuate to some extent due to the resonant operations. Thus, the theoretical gain characteristics slightly differed from the simulated ones. Hence, the simulation-based analysis is recommended to reinforce the theoretical analysis if precise gain characteristics in the entire frequency region are required.

The resonant tanks must be designed to ensure the gain requirement even if the input voltage fluctuates. An ordinary PFM feedback control system, similar to that for ordinary LLC converters, can regulate the output voltage

V. EXPERIMENTAL RESULTS
A. PROTOTYPE
A 1-kW prototype was designed and built for V_{in} = 400 V and V_{out} = 48 V, as shown in Fig. 10, and its component values are listed in Table 2. The resistances of primary and secondary windings, $r_{primary.j}$ and $r_{secondary.j}$, were measured by the frequency response analyzer (FRA5087, NF Corporation, Japan), and measured resistances at 106 kHz are shown in Table 2. As discussed in Section III-B, the three transformers Tr_A–Tr_C are preferably designed so that their parameters are matched to equalize peak currents of Phases A–C and to achieve high efficiency power conversion. In this paper, however, to verify the automatic capacitive current balancing capability, Tr_A–Tr_C were designed so that their key parameters of L_{mgj}, L_{kgj}, and n_j were intentionally severely mismatched.

Experiments with symmetric resonant operations were also performed to demonstrate the reduced conduction losses by the asymmetric resonant operations. C_1 and C_2 were replaced with ceramic capacitors with a capacitance of 4.4 μF so that these capacitors did not take part in resonant operations.

B. MEASURED WAVEFORMS
Measured currents of the primary windings, secondary windings, and an output port under the asymmetric resonant

TABLE 2. Component values.

Component	Value
Switches	Si MOSFET, STB45N65M5, R_{on} = 67 mΩ, C_{OSS} = 82 pF
Gate driver	ADuM3223ARZ
C_1 and C_2	Film capacitor, 470 nF, 13.8 mΩ
C_{rA}, C_{rB}, C_{rC}	Film capacitor, 680 nF, 10.1 mΩ
C_{bA}, C_{bB}, C_{bC}	Ceramic capacitor, 100 μF, 7.20 mΩ
C_{in}	Aluminum electrolytic capacitor, 94 μF, 63.0 mΩ
C_{out}	Ceramic capacitor, 32.9 μF, 1.00 mΩ
Diodes in full-wave rectifier	Schottky diode, V12P10-M3/86A, V_F = 0.580 V
Tr_A	n_A = 1.4, L_{kgA} = 2.29 μH, L_{mgA} = 30.5 μH, $r_{primary.A}$ = 70.8 mΩ, $r_{secondary.A}$ = 47.7 mΩ
Tr_B	n_B = 1.2, L_{kgB} = 2.20 μH, L_{mgB} = 23.1 μH, $r_{primary.B}$ = 64.8 mΩ, $r_{secondary.B}$ = 44.3 mΩ
Tr_C	n_C = 1.75, L_{kgC} = 3.07 μH, L_{mgC} = 30.8 μH, $r_{primary.C}$ = 93.7 mΩ, $r_{secondary.C}$ = 26.9 mΩ
f_{rAP}–f_{rCP}	f_{rAP} = 200 kHz, f_{rBP} = 257 kHz, f_{rCP} = 172 kHz
f_{rAN}–f_{rCN}	f_{rAN} = 128 kHz, f_{rBN} = 130 kHz, f_{rCN} = 110kHz
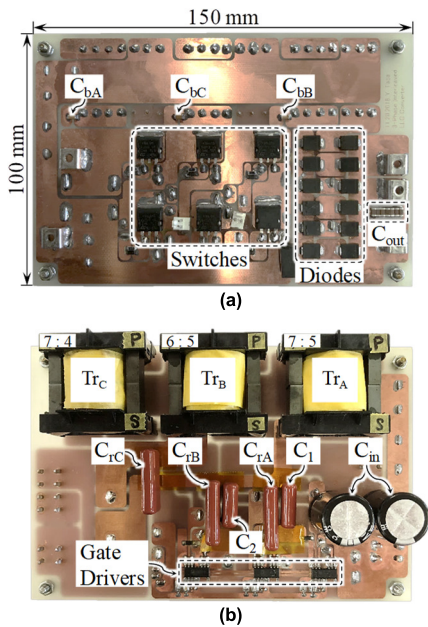
FIGURE 10. Photographs of 1-kW prototype: (a) front side, (b) rear side.

FIGURE 11. Measured current waveforms at 1 kW under asymmetric resonant operation: (a) i_A, i_B, and i_C, (b) i_{SA}, i_{SB}, and i_{SC}, (c)i_{rec} and I_{out}.

FIGURE 12. Measured current waveforms at 1 kW under symmetric resonant operation: (a) i_A, i_B, and i_C, (b) i_{SA}, i_{SB}, and i_{SC}, (c) i_{rec} and I_{out}.

operations at 1 kW and f_S = 106 kHz are shown in Figs. 11(a), (b), and (c), respectively. Despite the severely mismatched transformer parameters, the primary phase currents were automatically balanced, as shown in Fig. 11(a). The secondary phase currents, on the other hand, were slightly imbalanced due to the mismatch of each transformer's turn ratio, as shown in Fig. 11(b).

Figure 12 shows the measured current waveforms under the symmetric resonant operations at 1 kW and f_S = 145 kHz. The peak currents of the positive and negative half cycles of resonant tanks were nearly identical in the symmetric resonance, as shown in Figs. 12(a) and (b). With the asymmetric
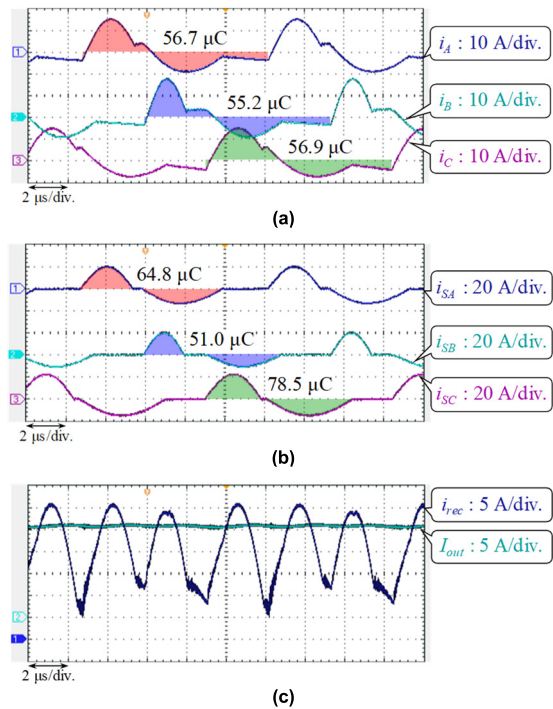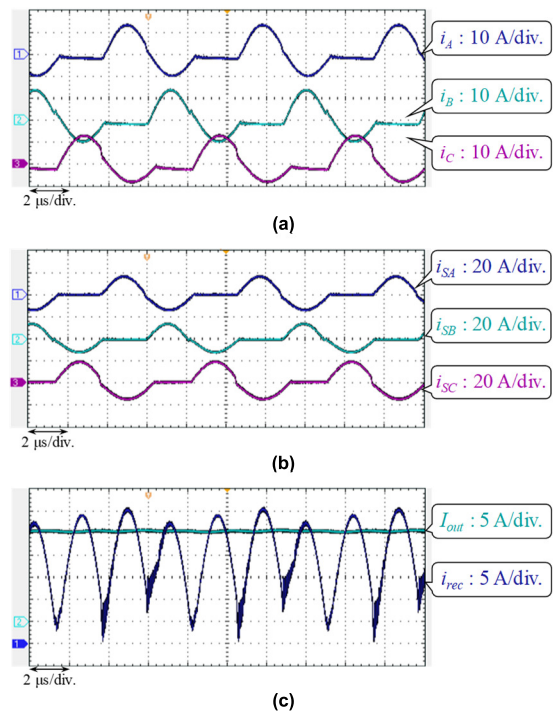
resonance [see Figs. 11(a) and (b)], on the other hand, the peak currents of the negative half-cycles were lower than those of the positive half cycles, reducing rms currents at a given output power.
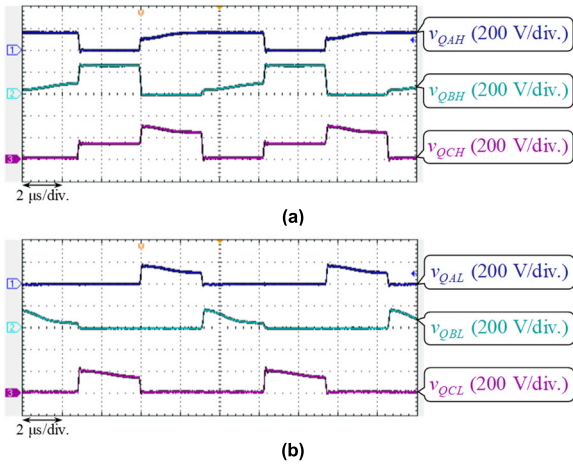
FIGURE 13. Measured voltage waveforms at 1 kW under asymmetric resonant operation: (a) high-side switches (Q_{AH}, Q_{BH}, and Q_{CH}) and (b) low-side switches (Q_{AL}, Q_{BL}, and Q_{CL}).

Measured voltage waveforms of the high- and low-sides switches at a full load of 1 kW under the asymmetric resonant operations are shown in Figs. 13(a) and (b), respectively. v_{QBH} and v_{QCH} were suppressed to around two-third of the input voltage, thanks to C_1 and C_2, as discussed in Section IV-B. Peak values of v_{QAH}, v_{QAL}, v_{QBL}, and v_{QCL} were suppressed to approximately one-third of V_{in}, though they slightly exceeded the theoretical values due to the resonances of C_1 and C_2.

Drain-source and gate-source voltages of the switches, v_{ds} and v_{gs}, at a full load of 1 kW under the asymmetric resonant operations are shown in Fig. 14. v_{gs} was applied after v_{ds} declined to zero, verifying ZVS turn-on for all switches. ZVS turn-off operations for all switches were also confirmed as v_{ds} rose with moderate dv/dt slope after v_{gs} dropped to zero.

C. AUTOMATIC CAPACITIVE CURRENT BALANCING

From the measured phase currents of the primary windings i_A–i_C, the averaged phase currents I_A–I_C were calculated from the following equation

$$I_j = \frac{1}{T_S} \int_0^{T_S} |i_j(t)| \, dt \qquad (43)$$

where j is A, B, or C.

The calculated I_A–I_C are shown in Fig. 15. Despite the severe mismatch in the transformers' parameters, I_A–I_C were automatically balanced with errors less than 2% over the entire output power range.

D. POWER CONVERSION EFFICIENCY

The measured and calculated power conversion efficiencies of the asymmetric and symmetric resonance are compared in Fig. 16. The peak efficiency of the symmetric resonance was as high as 92.4% at 700 W, and the full-load efficiency at 1 kW was 91.6%. With the asymmetric resonance, the efficiencies increased because of the lower rms values of i_A–i_C as well as reduced Joule losses. The full-load efficiency at
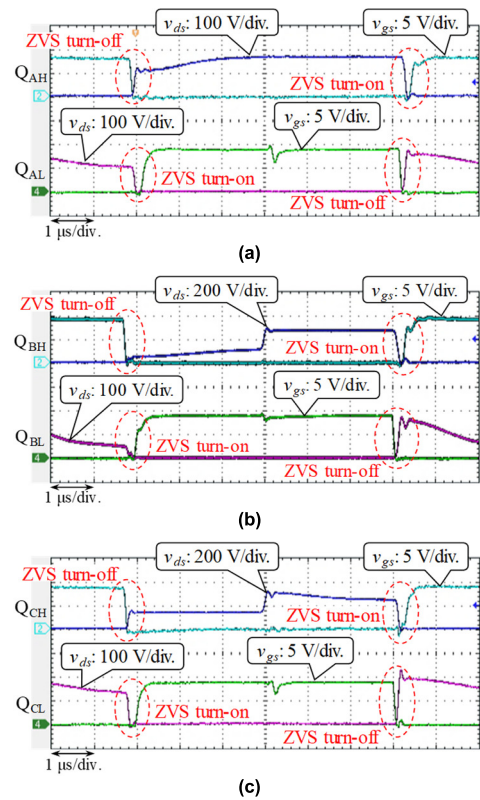

FIGURE 14. ZVS waveforms under asymmetric resonant operation: (a) Q_{AH} and Q_{AL}, (b) Q_{BH} and Q_{BL}, (c) Q_{CH} and Q_{CL}.
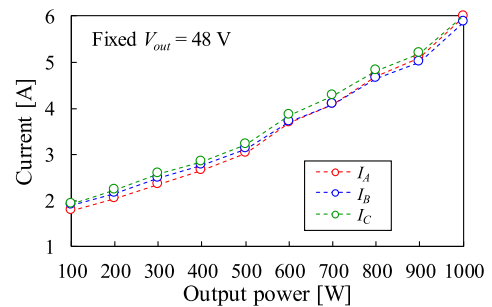

FIGURE 15. Measured phase currents of primary windings.

1 kW increased to as high as 93.1%, and the peak efficiency was 94.0% at 600 W.

The calculated power conversion efficiencies agreed very well with the measured ones, verifying the estimated loss breakdowns that will be shown in the next subsection.

E. LOSS ANALYSIS

Detailed loss breakdowns of the proposed interleaved LLC converter with the asymmetric or symmetric resonant operations were theoretically calculated. Figures 17(a) and (b) compare the estimated loss breakdowns at 500 W and 1 kW, respectively. Switching losses were assumed to be negligibly small due to ZVS operations over the entire output power range. Gate driving losses were excluded from these loss
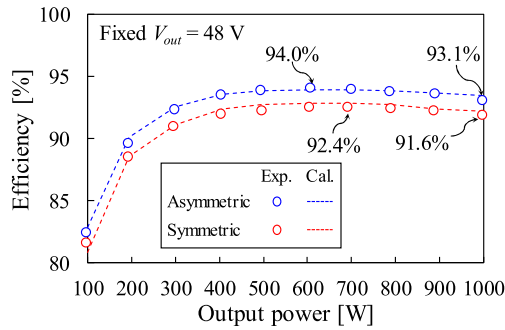
FIGURE 16. Measured and calculated power conversion efficiencies of asymmetric and symmetric resonance.
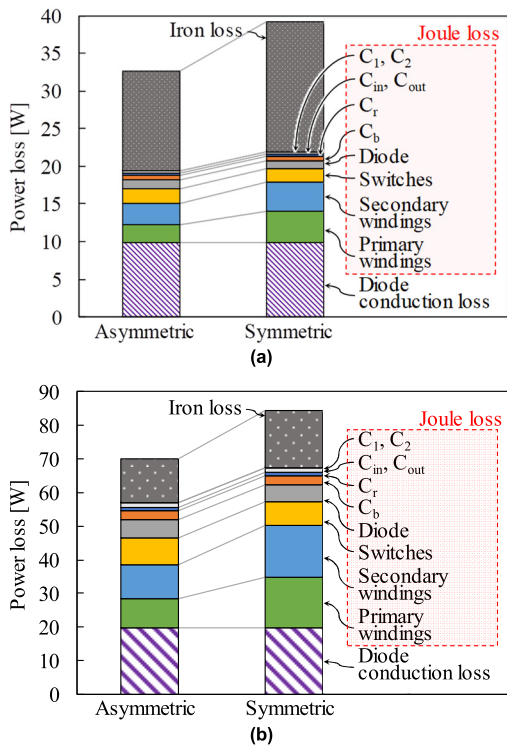

FIGURE 17. Comparison of estimated loss breakdowns of asymmetric and symmetric resonant operation at (a) 500 W and (b) 1 kW.

breakdowns since an auxiliary power supply drove the gate drivers. Iron losses of the transformers were experimentally measured and were obtained from no-load losses of the prototype.

It should be noted that there were slight differences in iron losses of the asymmetric and symmetric resonance because the switching frequency f_S slightly differed even at the same output power. To be specific, f_S of asymmetric resonant operations at 500 W and 1 kW were 123 and 106 kHz, respectively, whereas that of the symmetric resonant operations were 165 and 145 kHz.

The asymmetric resonant operation significantly reduced the Joule losses, especially the primary and secondary windings of the transformers (i.e., copper losses). Under both resonant operations, power losses in C_1 and C_2 were negligibly

small—the total loss in C_1 and C_2 was merely around 0.1 W at 1 kW.

Diode conduction losses were the dominant factors in both conditions of 500 W and 1 kW. Therefore, reducing the diode count by employing center-tapped transformers or synchronous rectifiers would effectively improve the efficiencies over the entire power range.

VI. CONCLUSION

This paper has proposed the three-phase interleaved LLC resonant converter with an automatic capacitive current balancing capability. Phase currents are automatically balanced by the flying capacitors without using current sensors nor feedback control loops, achieving the reduced circuit complexity and cost. The flying capacitors also contribute to lowering switches' voltage stresses. Furthermore, the proposed asymmetric resonant operations utilizing flying capacitors can reduce Joule losses of circuit components and copper losses of transformers.

The experimental verification using the 1-kW prototype demonstrated the automatic capacitive current balancing capability even with the severe mismatch in the transformers' parameters. The power conversion efficiency was improved thanks to the proposed asymmetric resonant operations compared to that of the symmetric ones.

REFERENCES

[1] H.-C. Chen, C.-Y. Lu, and U. S. Rout, "Decoupled master–slave current balancing control for three–phase interleaved boost converters," *IEEE Trans. Power Electron.*, vol. 33, no. 5, pp. 3683–3687, May 2018.

[2] K. I. Hwu and Y. H. Chen, "Applying differential–mode transformer to current sharing with current ripple considered," *IEEE Trans. Ind. Electron.*, vol. 58, no. 7, pp. 2755–2771, Jul. 2011.

[3] K. I. Hwu, W. Z. Jiang, and P. Y. Wu, "An expandable four–phase interleaved high step–down converter with low switch voltage stress and automatic uniform current sharing," *IEEE Trans. Ind. Electron.*, vol. 63, no. 10, pp. 6064–6072, Oct. 2016.

[4] M. Uno, M. Inoue, Y. Sato, and H. Nagata, "Bidirectional interleaved PWM converter with high voltage–conversion ratio and automatic current balancing capability for single–cell battery power system in small scientific satellites," *Energies*, vol. 11, no. 10, p. 2702, Oct. 2018.

[5] G. Yang, P. Dubus, and D. Sadarnac, "Double–phase high–efficiency, wide load range high- voltage/low–voltage LLC DC/DC converter for electric/hybrid vehicles," *IEEE Trans. Power Electron.*, vol. 30, no. 4, pp. 1876–1886, Apr. 2015.

[6] M. Noah, S. Kimura, J. Imaoka, W. Martinez, S. Endo, M. Yamamoto, and K. Umetani, "Magnetic design and experimental evaluation of a commercially available single integrated transformer in three–phase llc resonant converter," *IEEE Trans. Ind. Applicat.*, vol. 54, no. 6, pp. 6190–6204, Nov. 2018.

[7] E. Orietti, P. Mattavelli, G. Spiazzi, C. Adragna, and G. Gattavari, "Two-phase interleaved LLC resonant converter with current-controlled inductor," in *Proc. Brazilian Power Electron. Conf.*, Sep. 2009, pp. 298–304.

[8] Z. Hu, Y. Qiu, L. Wang, and Y.-F. Liu, "An interleaved LLC resonant converter operating at constant switching frequency," *IEEE Trans. Power Electron.*, vol. 29, no. 6, pp. 2931–2943, Jun. 2014.

[9] Z. Hu, Y. Qiu, Y.-F. Liu, and P. C. Sen, "A control strategy and design method for interleaved LLC converters operating at variable switching frequency," *IEEE Trans. Power Electron.*, vol. 29, no. 8, pp. 4426–4437, Aug. 2014.

[10] H. Wang, Y. Chen, Y. Qiu, P. Fang, Y. Zhang, L. Wang, Y.-F. Liu, J. Afsharian, and Z. Yang, "Common capacitor multiphase LLC converter with passive current sharing ability," *IEEE Trans. Power Electron.*, vol. 33, no. 1, pp. 370–387, Jan. 2018.

[11] H. Wang, Y. Chen, Y.-F. Liu, J. Afsharian, and Z. Yang, "A passive current sharing method with common inductor multiphase LLC resonant converter," *IEEE Trans. Power Electron.*, vol. 32, no. 9, pp. 6994–7010, Sep. 2017.

[12] M. Noah, S. Endo, H. Ishibashi, K. Nanamori, J. Imaoka, K. Umetani, and M. Yamamoto, "A current sharing method utilizing single balancing transformer for a multiphase LLC resonant converter with integrated magnetics," *IEEE J. Emerg. Sel. Topics Power Electron.*, vol. 6, no. 2, pp. 977–992, Jun. 2018.

[13] O. Kirshenboim and M. M. Peretz, "Combined multilevel and two–phase interleaved LLC converter with enhanced power processing characteristics and natural current sharing," *IEEE Trans. Power Electron.*, vol. 33, no. 7, pp. 5613–5620, Jul. 2018.

[14] X. Fang, H. Hu, Z. J. Shen, and I. Batarseh, "Operation mode analysis and peak gain approximation of the LLC resonant converter," *IEEE Trans. Power Electron.*, vol. 27, no. 4, pp. 1985–1995, Apr. 2012.

[15] G. Ivensky, S. Bronshtein, and A. Abramovitz, "Approximate analysis of resonant LLC DC–DC converter," *IEEE Trans. Power Electron.*, vol. 26, no. 11, pp. 3274–3284, Nov. 2011.

[16] X. Sun, Y. Shen, Y. Zhu, and X. Guo, "Interleaved boost–integrated LLC resonant converter with fixed–frequency PWM control for renewable energy generation applications," *IEEE Trans. Power Electron.*, vol. 30, no. 8, pp. 4312–4326, Aug. 2015.

[17] X. Sun, Y. Shen, W. Li, and H. Wu, "A PWM and PFM hybrid modulated three–port converter for a standalone PV/battery power system," *IEEE J. Emerg. Sel. Topics Power Electron.*, vol. 3, no. 4, pp. 984–1000, Dec. 2015.

MASATOSHI UNO (Member, IEEE) was born in Japan, in 1979. He received the B.E. degree in electronics engineering and the M.E. degree in electrical engineering from Doshisha University, Kyoto, Japan, in 2002 and 2004, respectively, and the Ph.D. degree in space and astronautical science from the Graduate University for Advanced Studies, Hayama, Japan, in 2012.

In 2004, he joined the Japan Aerospace Exploration Agency, Sagamihara, Japan, where he developed spacecraft power systems including battery, photovoltaic, and fuel cell systems. In 2014, he joined the Department of Electrical and Electronics Engineering, Ibaraki University, Ibaraki, Japan, where he is currently an Associate Professor of electrical engineering. His research interests include switching power converters for renewable energy systems, life evaluation for EDLCs and lithium-ion batteries, and the development of spacecraft power systems. He received the Isao Takahashi Power Electronics Award, in 2018.

YOSHIYA TADA was born in 1994. He received the B.E. degree in electrical and electronics engineering from Ibaraki University, Hitachi, Japan, where he is currently pursuing the M.E. degree in electrical and electronics engineering with the Graduate School of Science and Engineering.

His research interest includes resonant converters.

YUSUKE SATO was born in 1995. He received the B.E. and M.S. degrees in electrical and electronics engineering from Ibaraki University, Ibaraki, Japan, in 2017 and 2019, respectively. He is currently with Panasonic Corporation. His research interest includes dc–dc converters for automotive applications.

• • •